

Investigation of the quasifission process by theoretical analysis of experimental data of fissionlike reaction products

G Giardina^{1,2}, A K Nasirov^{3,4}, G Mandaglio^{1,2}, F Curciarello^{1,2},
V De Leo^{1,2}, G Fazio^{1,2}, M Manganaro^{1,2}, M Romaniuk^{1,2}, C Saccá⁵

¹ Dipartimento di Fisica, Università di Messina, I-98166 Messina, Italy

² Istituto Nazionale di Fisica Nucleare, Sezione di Catania, I-95123 Catania, Italy

³ Joint Institute for Nuclear Research, 141980, Dubna, Russia

⁴ Institute of Nuclear Physics, 100214, Tashkent, Uzbekistan

⁵ Dipartimento di Scienze della Terra, Università di Messina, I-98166 Messina, Italy

E-mail: giardina@nucleo.unime.it

Abstract. The fusion excitation function is the important quantity in planning experiments for the synthesis of superheavy elements. Its values seem to be determined by the experimental study of the hindrance to complete fusion by the observation of mass, angular and energy distributions of the fissionlike fragments. There is ambiguity in establishment of the reaction mechanism leading to the observed binary fissionlike fragments. The fissionlike fragments can be produced in the quasifission, fast fission, and fusion-fission processes which have overlapping in the mass (angular, kinetic energy) distributions of fragments. The branching ratio between quasifission and complete fusion strongly depends on the characteristics of the entrance channel. In this paper we consider a wide set of reactions (with different mass asymmetry and mass symmetry parameters) with the aim to explain the role played by many quantities on the reaction mechanisms. We also present the results of study of the $^{48}\text{Ca}+^{249}\text{Bk}$ reaction used to synthesize superheavy nuclei with $Z = 117$ by the determination of the evaporation residue cross sections and the effective fission barriers $< B_f >$ of excited nuclei formed along the de-excitation cascade of the compound nucleus.

1. Introduction

The experimental and theoretical investigations of reaction dynamics connected with the formation of composed system is nowadays the main subject of the nuclear reactions. At the first stage of reaction of heavy ion collisions the full momentum transfer can occur (this event is defined as capture) if there is a well in the nucleus-nucleus potential in dependence on the values of relative kinetic energy and friction coefficients [1,2]. At capture, the two reacting nuclei form a rotating nuclear system at near Coulomb barrier energies. During its evolution this system can be transformed into compound nucleus or it re-separates into two fragments which may differ from the initial nuclei in the entrance channel [3–5]. During the evolution of DNS its two nuclei may change their masses A_1 , A_2 and charges Z_1 , Z_2 but with constant total mass $A = A_1 + A_2$ and charge $Z = Z_1 + Z_2$. The DNS should overcome the intrinsic fusion barrier B_{fus}^* (it is equal to the difference between the maximum value of the driving potential and its value

corresponding to the initial charge asymmetry) to reach the compound nucleus state through more mass asymmetric configurations. The intense of the break up of DNS into two nuclei (quasifission channel) in competition with the complete fusion is characterized by the value of the quasifission barrier B_{qf} (the depth of the pocket in the nucleus-nucleus potential) [1,2]. The mass asymmetry parameter of quasifission fragments may be larger or smaller than that of nuclei in the entrance channel. It is well known the case of the quasifission with small mass asymmetry in comparison with one of initial nuclei. In this case the maximum of the mass distribution of quasifission fragments places between the masses of projectile (or target) and symmetric fission fragments.

On the other hand, due to the exchange with neutrons and protons between the nuclei constituting the DNS the mass asymmetry parameter increases being larger than the mass asymmetry in the entrance channel (evolution to complete fusion direction) and at the same time there is also a relevant probability of DNS to decay into two nuclei. The decay probability depends on the excitation energy and quasifission barrier B_{qf} of DNS at a given configuration. Of course, the mass distribution of quasifission products are related to the characteristics of the entrance channel (beam energy and orientation angles of the axial symmetry axis of reacting nuclei).

The capture events surviving quasifission populate the complete fusion channel. Consequently, the deformed mononucleus may reach the fully equilibrated statistical shape of the compound nucleus (CN), or if there is no the fission barrier B_{f} the system immediately decays into two fragments (fast fission process). The latter phenomenon occurs only at high angular momentum ℓ for which the fission barrier of the complete fusion system disappears ($B_{\text{f}}(\ell > \ell_{\text{f}}) = 0$). Therefore, the fast fission process takes place only in the reactions at high angular momentum values ($\ell > \ell_{\text{f}}$) while the quasifission process takes place at all values of ℓ contributing to the capture reaction.

Finally, in the last stage of nuclear reaction, the formed CN may de-excite by emission of light particles or undergoes to fission (producing fusion-fission fragments). The reaction products that survive fission are the evaporation residues (ER) [6,7]. The registration of ER is clear evidence of the compound nucleus formation, but generally the determination of ER's only it is not enough to determine the complete fusion cross section and to understand the dynamics of the de-excitation cascade of CN if the fission fragments are not included into consideration. On the other hands, it is difficult for sure correct determination of the fusion-fission rate in the cases of overlapping of the mass and angle distributions of the products of different processes (quasifission, fast fission and fusion-fission) because sorting out the registered fissionlike fragments according to the mechanism of its origin is connected with some assumptions.

Moreover, by observing the fission products of fissile nuclei formed in the in neutron (or very light particles)-induced reactions with the heavy targets one can conclude that the low excited compound nucleus (at about $E_{\text{CN}}^* < 10$ MeV) decays into very asymmetric fission fragments (near to the shell closure), while the compound nuclei formed in heavy ion collisions at intermediate or high excitation energy ($E_{\text{CN}}^* > 20$ MeV) undergo fission forming the mass symmetric fragments. Starting from these general observations some researchers put forward the idea that the complete fusion process of two colliding nuclei may be considered as the inverse process to fission. The authors of the papers [8,9] argued that since the fission of a compound nucleus in heavy ion collisions produces just symmetric fragments, then in the collisions of two symmetric (or almost symmetric) nuclei complete fusion has to be a very probable process. But, unfortunately this is not true. For systems of colliding nuclei heavier than $^{110}\text{Pd}+^{110}\text{Pd}$ the fusion does not occur absolutely, while for the reactions like $^{100}\text{Mo}+^{100}\text{Mo}$, $^{96}\text{Zr}+^{96}\text{Zr}$, $^{96}\text{Zr}+^{100}\text{Mo}$, $^{100}\text{Mo}+^{110}\text{Pa}$ or induced by projectiles higher than Zn, Ge, Kr there is a strong hindrance to fusion.

Following the previous reasons one can affirm that the hypothetical $^{132}\text{Sn}+^{120}\text{Cd}$ reaction

should lead to the ^{252}Cf CN since ^{120}Cd (with $Z=48$ near the shell closure 50) and ^{132}Sn (with double shell closure $Z=50$ and $N=82$) are produced with highest yields in spontaneous fission of ^{252}Cf . But our estimation for this reaction does not give meaningful fusion probability ($P_{\text{CN}} < 5 \times 10^{-7}$).

The simple reason resides in the peculiarities of the reaction dynamics. In the spontaneous fission of ^{252}Cf the average value of angular momentum distribution of the fragments is close to zero, but if we want to reach the ^{252}Cf compound nucleus, by the hypothetical $^{132}\text{Sn}+^{120}\text{Cd}$ reaction (or by the realistic $^{132}\text{Sn}+^{116}\text{Cd}$ reaction leading to the ^{248}Cf CN), the average value of angular momentum distribution of DNS in the entrance channel may be about $\langle \ell \rangle = 50\hbar$ or higher by increasing the beam energy. The $\langle \ell \rangle$ value is calculated as

$$\langle \ell (E_{\text{c.m.}}; \alpha_P, \alpha_T) \rangle = \frac{\sum_{\ell=0}^{\ell=\ell_d} \ell < \sigma_{(\text{cap})}^{(\ell)} >_{\alpha_P, \alpha_T} (E_{\text{c.m.}})}{\sum_{\ell=0}^{\ell=\ell_d} < \sigma_{(\text{cap})}^{(\ell)} >_{\alpha_P, \alpha_T} (E_{\text{c.m.}})} . \quad (1)$$

In the fusion reaction mechanism, at the first stage, DNS which is formed after capture of projectile by the target nuclei should survive quasifission (re-separation of nuclei of DNS). Due to the hindrance connected with quasifission for these system the fusion probability P_{CN} should be lower than 10^{-7} for small values of angular momentum. This low probability of complete fusion becomes more lower for the excited and fast rotating deformed mononucleus which undergoes fast fission before the system can reach the compact shape of compound nucleus.

Also in the cases of the explored $^{22}\text{Ne}+^{250}\text{Cf}$ (more mass asymmetric system), $^{24}\text{Mg}+^{248}\text{Cm}$, $^{28}\text{Si}+^{244}\text{Pu}$, $^{34}\text{S}+^{238}\text{U}$, and $^{40}\text{Ar}+^{232}\text{Th}$ (less mass asymmetric system) reactions, the compound nucleus ^{272}Hs is formed with different angular momentum distributions in dependence on entrance channels even the defined excitation energy E_{CN}^* has been achieved. Therefore, such compound nuclei decay by different yields of reaction products. The fusion-fission fragment mass distributions are peaked at around the ^{136}Xe nucleus with different dispersions and average angular momentum distributions in connection with the various entrance channels. If we calculate the formation probability of the ^{272}Hs compound nucleus in the mass symmetric $^{136}\text{Xe}+^{136}\text{Xe}$ reaction at the same fixed excitation energy E_{CN}^* as in the considered $^{22}\text{Ne}+^{250}\text{Cf}$ reaction (where $P_{\text{CN}} \simeq 1$), we do not meaningfully reach such a compound nucleus ($P_{\text{CN}} < 10^{-10}$). The angular momentum distribution for the $^{136}\text{Xe}+^{136}\text{Xe}$ collision at the capture stage is completely different and all conditions of reaction dynamics lead to deep inelastic and quasifission products.

In this context, for the $^{136}\text{Xe}+^{132}\text{Sn}$ ($P_{\text{CN}} < 10^{-8}$) and $^{132}\text{Sn}+^{176}\text{Yb}$ ($P_{\text{CN}} < 5 \times 10^{-11}$) reactions, one can observe the same above-described hindrance to complete fusion.

2. Capture and Deep Inelastic Collision

Our theoretical capture cross section σ_{cap} includes all damped reactions, excluding deep inelastic collisions (DIC). The partial capture cross sections are contributed by the full momentum transfer events corresponding to the trapping into a pocket in the nucleus-nucleus potential after dissipation of the relative kinetic energy. Differently, the DIC events are not characterized by the full momentum transfer and collision paths are not trapped in the pocket of the nucleus-nucleus potential. The DIC events are not connected with any pocket of a potential; for example at large values of ℓ there is no pocket but the DIC events take place. The partial capture cross section is calculated by the following formula

$$\sigma_{\text{cap}}^{\ell}(E_{\text{c.m.}}) = \pi \lambda^2 \mathcal{P}_{\text{cap}}^{\ell}(E_{\text{c.m.}}) \quad (2)$$

with the capture probability $\mathcal{P}_{\text{cap}}^{\ell}$ which is found by the solution of the motion equations [10, 11].

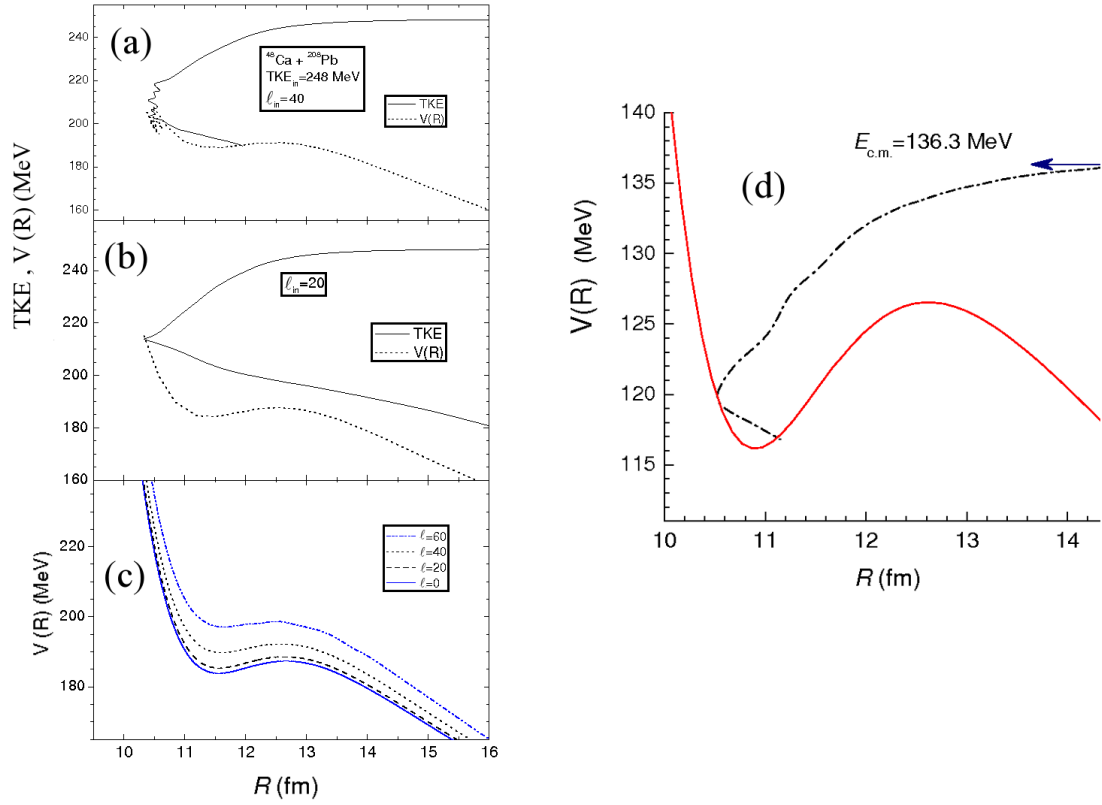


Figure 1. Capture (a) and deep inelastic collision (b) for the $^{48}\text{Ca} + ^{208}\text{Pb}$ reaction. Dependence of nucleus-nucleus potential (c) on the orbital angular momentum ℓ . Illustration of capture path (d) (dot dashed line) into potential well (solid line) as obtained by the numerical solution of the equation of relative motion of colliding nuclei with the initial energy $E_{\text{c.m.}} = 136.3$ MeV and $\ell = 0$ for the $^{32}\text{S} + ^{184}\text{W}$ reaction [2].

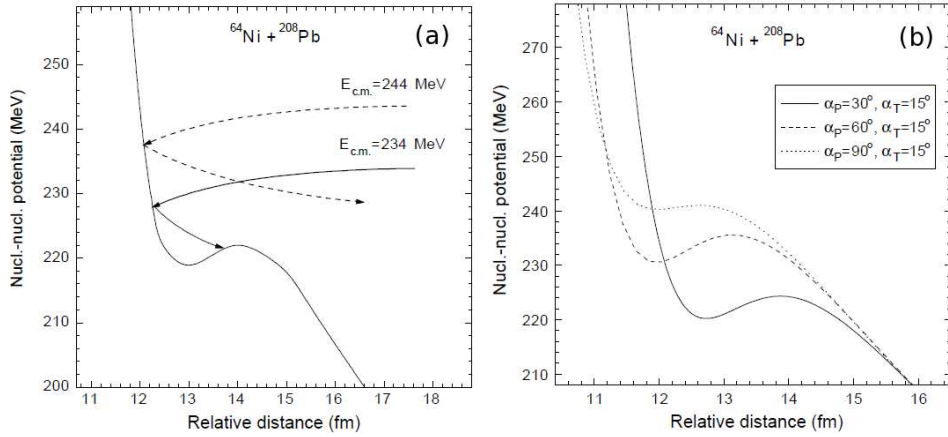


Figure 2. (a) Dependence of capture (solid curve) and deep inelastic collision (dashed curve) processes for nucleus-nucleus collisions on the internuclear potential $V(R)$ and on the initial values of the beam energy $E_{\text{c.m.}}$. (b) Dependence of the nucleus-nucleus potential on the mutual orientation of colliding nuclei; solid line: $\alpha_1 = 30^\circ$ and $\alpha_2 = 15^\circ$; dashed line: $\alpha_1 = 60^\circ$ and $\alpha_2 = 15^\circ$; dotted line: $\alpha_1 = 90^\circ$ and $\alpha_2 = 15^\circ$.

In the calculation of nucleus-nucleus potential, which includes the Coulombian $V_{\text{Coul}}(Z, A, R)$, nuclear $V_{\text{n}}(Z, A, R)$ and rotational $V_{\text{rot}}(Z, A, R, \ell)$ parts, we take into account the static and dynamic deformations, and orientation angles of the axial symmetry axes of reacting nuclei, at initial stage.

In Fig. 2 we present an example of capture events with different potential wells and its dependencies on the angular momentum and orientation angles of axes of reacting nuclei; moreover, in figures we also present the cases of capture and DIC events by changing the beam

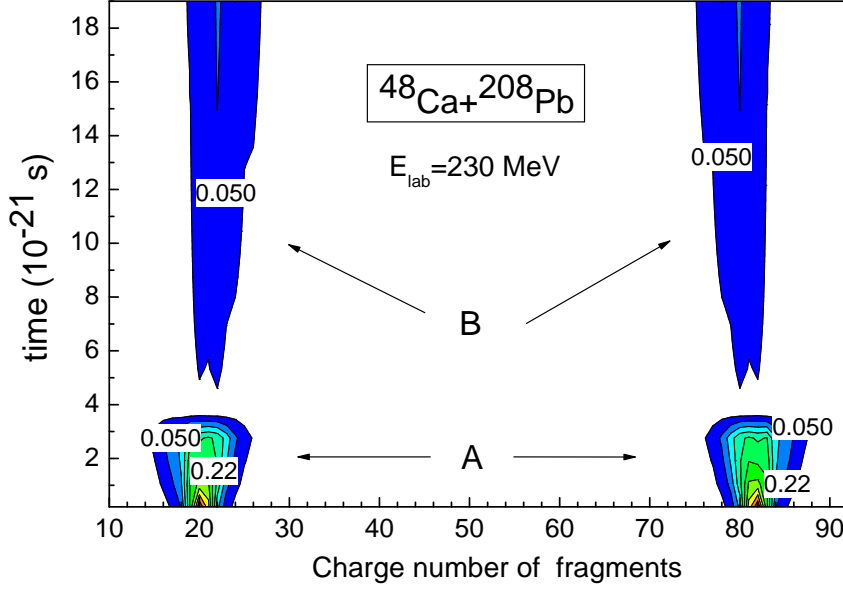


Figure 3. Time dependence of the theoretical results for the mass distribution of the deep inelastic collision (A) and quasi-fission (B) fragments in the $^{48}\text{Ca}+^{208}\text{Pb}$ reaction.

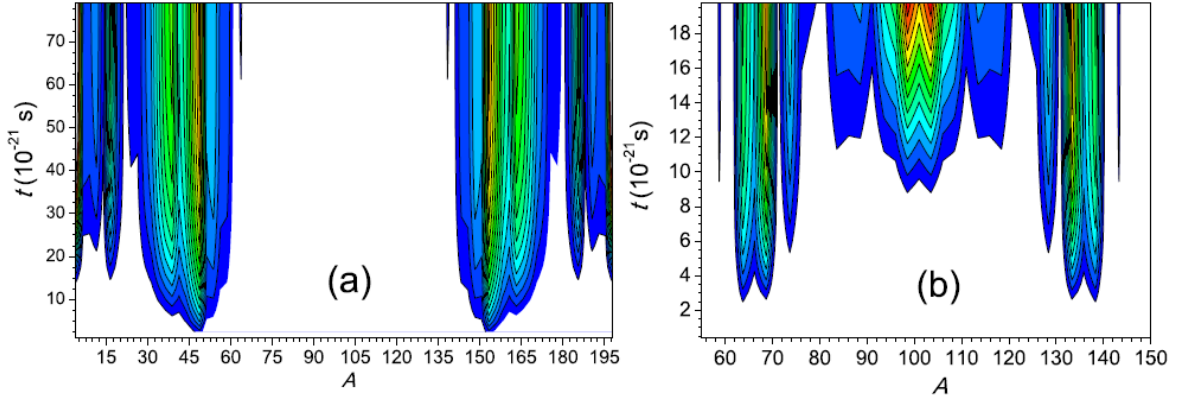


Figure 4. The mass distribution of the quasifission product yields obtained in the $^{48}\text{Ca}+^{154}\text{Sm}$ reaction at $E_{c.m.}=140$ MeV (panel (a)) and $E_{c.m.}=160$ MeV (panel (b)) as a function of the lifetime of the dinuclear system formed at capture stage.

energies and angular momentum values.

The lifetime of an excited DNS for a given reaction depends on the initial collision energy $E_{c.m.}$ and angular momentum distribution values (see formulae (6)-(8) and Fig.4 of our paper [12]). The mass and charge, as well as shapes of nuclei constituting the DNS are changed during interaction time. The evolution of DNS depends on its excitation energy, orientation angles of the axial symmetry axes and shell structures of reacting nuclei. During its evolution DNS can evolve to complete fusion or can decay into two fragments (quasifission process). The competition between these two processes is related to the values of intrinsic fusion barrier B_{fus}^* and quasifission barrier B_{qf} [2,6,7] depending on the peculiarities of reacting nuclei, beam energy and angular momentum distribution.

In many cases and conditions the mass and angular momentum distributions of quasifission fragments can overlap with the mass and angular distributions of fusion-fission fragments, or/and with the ones of the fast fission fragments [10, 13], leading to the real difficulties in the experimental analysis in order to sort out the true yields of fragments belonged to various reaction mechanisms (see for example [10, 14] and Fig. 3 of Ref. [15]).

Usually, in reactions with actinides the maximum of the yield of the quasifission products is observed in the mass region between masses of the projectile-like products and symmetric

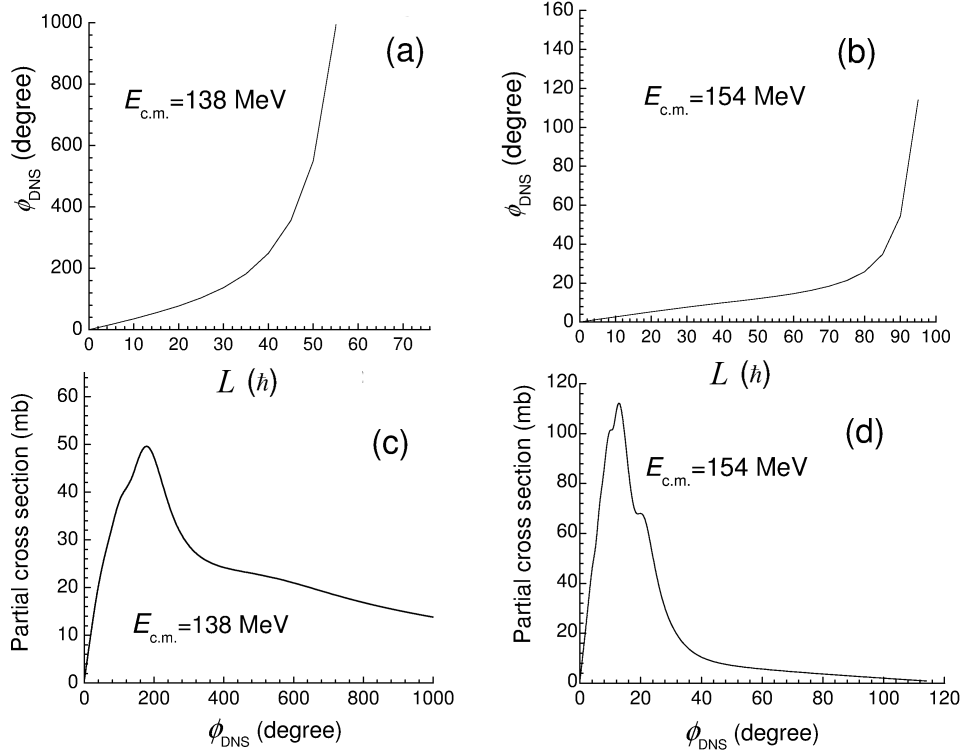


Figure 5. The rotation angle ϕ_{DNS} of the dinuclear system forming the ^{58}Cr and ^{144}Ce fragments (reached by the $^{48}\text{Ca}+^{154}\text{Sm}$ reaction at two different beam energies) as a function of the orbital angular momentum L in (a) and (b), and the angular distributions of the quasifission ^{58}Cr and ^{144}Ce fragments at decay of DNS in (c) and (d).

masses. In the $^{48}\text{Ca} + ^{208}\text{Pb}$ reaction, the maximum of the quasifission products is very close to the region of projectilelike and targetlike fragments (see Fig. 3 of Ref. [10], as well as Fig. 1 of Ref. [16] and Fig. 8 of Ref. [17]). This is due to the fact that projectile and target are double magic nuclei. As a result the mass distributions of the capture, *i.e.* quasifission reactions, and deep inelastic collisions are mixed. The reaction time of the deep inelastic collisions is much smaller than that of quasifission and fast fission reactions, because the last two reactions take place if capture occurs, *i.e.* projectile has been trapped into potential well (see Fig. 1).

It is difficult to separate without uncertainty products of these two processes in experimental data. To demonstrate the importance of this circumstance, the mass distributions of the deep-inelastic and capture reactions were calculated by the method developed on the basis of the DNS concept [18, 19]. The results for the $^{48}\text{Ca}+^{248}\text{Pb}$ reaction are presented in Fig. 3. The reason of this result can be seen from the driving potential which has a deep valley around initial charge asymmetry due to the nuclear shell effects. Therefore, the sufficient part of the yields of quasifission and deep-inelastic products are mixed in the mass and charge distributions. The difference between them is in their angular distributions which are connected with the lifetime of the formed rotated DNS. The overlap of the maximum of the mass distribution of quasifission with that of the deep inelastic collisions can lead to conclusion that there is no the contribution of the quasifission process in the total reaction cross section. This explains the strong deviation of the theoretical values of the capture cross section at low energies from the experimental capture cross section which was determined by the symmetric fragmentation only.

So, the mixing of the mass distributions of the deep inelastic collisions and quasifission processes causes an ambiguous determination of the capture cross section from the experimental mass distributions in case of reactions with magic or double magic nuclei, like to the case of the reaction under discussion. As well as the mixing of the mass distributions of the quasifission,

fast fission and fusion-fission reactions makes difficult the estimation of the complete fusion cross section leading to the genuine compound nucleus. Due to the strong dependence of the mass distribution on the peculiarities of nuclear shell structure, the proportion of mixing is changed from one reaction to another reaction. The theoretical study of this problem is useful to establish the reactions and beam energies which are favorable to obtain the maximum cross section of formation of the compound nucleus with the relatively low angular momentum and excitation energy.

We can state that, at the low energies, the products of the symmetric fragmentation in the $^{48}\text{Ca}+^{208}\text{Pb}$ reaction are generally formed at usual fission of CN, and therefore they are related to the fusion cross section. At energies $E_{lab} > 212$ MeV the contribution of the fast fission appears and it increases by the beam energy. That will be shown in Fig. 8.

Moreover, Fig. 4 shows the mass distribution of the quasifission products of the $^{48}\text{Ca}+^{154}\text{Sm}$ reaction as a function of the DNS lifetime, following the capture reaction at two $E_{c.m.}$ energies of 140 MeV (panel (a)) and 160 MeV (panel (b)). At lower energies (panel (a)) the mass distribution of quasifission fragments are asymmetric; at higher beam energy (panel (b)), also appear mass symmetric quasifission fragments. The latter mass distribution of quasifission fragments overlap to the fusion-fission mass distribution leading to a relevant uncertainty in experimental determination of the fusion cross section.

In Fig. 5 we present the results of the $^{48}\text{Ca}+^{154}\text{Sm}$ reaction regarding the determination of the rotational angle ϕ_{DNS} of the dinuclear system at two $E_{c.m.}$ beam energies of 138 and 154 MeV (see panels (a) and (b), respectively) versus the angular momentum L values of DNS, and the angular distributions of the quasifission ^{58}Cr and ^{144}Ce fragments at decay of DNS for the energies $E_{c.m.}=138$ and 154 MeV, (see panels (c) and (d), respectively). As one can see, at $E_{c.m.}=138$ MeV the decay of DNS into the two mentioned fragments lead to large rotational angle ϕ_{DNS} at intermediate and high angular momentum components (panel (a)) as well as a wide angular distributions of the quasifission ^{58}Cr and ^{144}Ce fragments at all DNS rotational angles (panel (c)); while, at high energy $E_{c.m.}=154$ MeV, the rotational angle ϕ_{DNS} is small up to large angular momentum values (panel (b)), and the angular distribution of the quasifission fragments is strongly peaked to low rotational angle values of DNS (panel(d)). This means that at $E_{c.m.}=138$ MeV for $L > 35\hbar$ the rotation angle is enough large and the angular distribution of the quasifission fragments may be nearly isotropic. The maximum of the angular distribution moves to small angles at larger energies: $E_{c.m.}=154$ MeV the most part of fragments is distributed to the forward angles and to backward angles for the relative fragment-partner (see panel (d)), and the maximum of the angular distribution are concentrated around $\phi_{DNS} = 15^\circ$ in the center-of-mass system. Therefore the large part of quasifission fragments passes beside the nearest to the beam detector. This phenomenon caused the conclusions of the authors of Ref. [20] about decreasing of quasifission events at energies $E_{c.m.} > 154$ MeV. The reason of decreasing in the experimental events of quasifission at low energies $E_{c.m.} < 138$ MeV is the isotropic angular distribution of some part of quasifission fragments which were considered as the compound nucleus fission fragments.

3. Evolution of DNS : competition between quasifission and complete fusion processes

The composite system formed at capture stage evolves by exchanging nucleons between the two nuclei constituting the DNS. During its evolution the DNS can reach the shape of a deformed mononucleus (complete fusion) or it can break up into two fragments (quasifission) without reaching the complete fusion stage. In the first case the nuclear system has to reach the statistical equilibrate shape of the CN with the angular momentum ℓ_{CN} . The equilibrium shape of compound nucleus depends on the value of ℓ_{CN} which determines the fission barrier B_f providing its stability against to fission. It is well known that $B_f=0$ if the value of ℓ_{CN} is

larger than its critical value $\ell > \ell_f$ for the compound nucleus with the given mass and charge number [21]. Therefore, the events of complete fusion for $\ell > \ell_f$ cannot reach the equilibrium shape of CN because the mononucleus immediately decays into two fragments. This fissionlike process is called fast fission because compound nucleus is not formed. Competition between complete fusion and quasifission occurs at all values of the orbital angular momentum. Therefore, the partial capture cross section is contributed by the following terms:

$$\sigma_{cap}^{\ell}(E_{c.m.}; \beta_P, \alpha_T) = \sigma_{qfiss}^{\ell}(E_{c.m.}; \beta_P, \alpha_T) + \sigma_{fus}^{\ell}(E_{c.m.}; \beta_P, \alpha_T) + \sigma_{fastfis}^{\ell}(E_{c.m.}; \beta_P, \alpha_T) \quad (3)$$

where

$$\sigma_{fus}^{\ell}(E_{c.m.}) = \sigma_{cap}^{\ell}(E_{c.m.})P_{CN}(E_{c.m.}, \ell), \quad (4)$$

is the partial fusion cross section and $P_{CN}(E_{c.m.}, \ell)$ is fusion probability as a function of ℓ . It is clear that the fusion cross section in formula (4) includes the cross sections of evaporation residue and fusion-fission products. The fusion cross section, for each orientation angles of the symmetry axes of the deformed reacting nuclei, is obtained by formula

$$\sigma_{fus}(E_{c.m.}; \beta_P, \alpha_T) = \sum_{\ell=0}^{\ell_f} (2\ell + 1) \sigma_{cap}(E_{c.m.}, \ell; \beta_P, \alpha_T) P_{CN}(E_{c.m.}, \ell; \beta_P, \alpha_T). \quad (5)$$

Therefore, taking into account the contributions of all configurations with the orientation angles of the symmetry axes of the deformed reacting nuclei we can calculate the averaged value of the fusion cross section by formula:

$$\langle \sigma_{fus} \rangle_{\{\alpha_P, \alpha_T\}}(E_{c.m.}) = \int_0^{\pi/2} \sin \alpha_P \int_0^{\pi/2} \sin \alpha_T \times \sigma_{fus}(E_{c.m.}; \alpha_P, \alpha_T) d\alpha_T d\alpha_P, \quad (6)$$

when both nuclei are deformed nuclei, or by formula:

$$\langle \sigma_{fus} \rangle_{\{\alpha_T\}}(E_{c.m.}) = \int_0^{\pi/2} \sin \alpha_T \times \sigma_{fus}(E_{c.m.}; \alpha_T) d\alpha_T, \quad (7)$$

for the spherical projectile and deformed target.

Obviously, the quasifission cross section is obtained as

$$\sigma_{qfis}(E_{c.m.}; \beta_P, \alpha_T) = \sum_{\ell=0}^{\ell_d} (2\ell + 1) \sigma_{cap}(E_{c.m.}, \ell; \beta_P, \alpha_T) (1 - P_{CN}(E_{c.m.}, \ell; \beta_P, \alpha_T)), \quad (8)$$

where ℓ_d is the maximum value of ℓ at which the capture events occur.

Another binary process which leads to the formation of two fragments similar to the ones of fusion-fission or quasifission is the fast fission. The fast fission cross section is calculated by summing the contributions of the partial cross sections related to the range $\ell_f \leq \ell \leq \ell_d$ (for which $B_f=0$) leading to the formation of the mononucleus:

$$\sigma_{fastfis}(E_{c.m.}; \beta_P, \alpha_T) = \sum_{\ell_f}^{\ell_d} (2\ell + 1) \sigma_{cap}(E_{c.m.}, \ell; \beta_P, \alpha_T) P_{CN}(E_{c.m.}, \ell; \beta_P, \alpha_T). \quad (9)$$

The fission and the evaporation residue cross sections are calculated by the advanced statistical code [1, 6, 10] that takes into account the damping of the shell correction in the fission barrier as a function of nuclear temperature and orbital angular momentum.

3.1. Calculation of competition between quasifission and complete fusion processes

The fusion cross section is calculated from the branching ratio $P_{\text{CN}}(Z)$ of the decay rates of overflowing the border of the potential well ($B_{\text{qf}}^{(Z)}$) along R at a given mass asymmetry (decay of DNS in quasifission fragments) over the barriers on mass asymmetry axis B_{fus}^* for the complete fusion or $B_{\text{sym}}^{(Z)}$ in opposite direction to the symmetric configuration of DNS (for details see Fig. 4 of Ref. [2]):

$$P_{\text{CN}}^{(Z)}(E_{\text{DNS}}^*) \approx \frac{\Gamma_{\text{fus}}^{(Z)}(B_{\text{fus}}^*, E_{\text{DNS}}^*)}{\Gamma_{(\text{qf})}^{(Z)}(B_{\text{qf}}, E_{\text{DNS}}^*) + \Gamma_{(\text{fus})}^{(Z)}(B_{\text{fus}}^*, E_{\text{DNS}}^*) + \Gamma_{\text{sym}}^{(Z)}(B_{\text{sym}}, E_{\text{DNS}}^*)}, \quad (10)$$

where Γ_{fus} , Γ_{qf} and Γ_{sym} are corresponding widths determined by the level densities on the barriers B_{fus}^* , B_{sym}^* and B_{qf} involved in the calculation of P_{CN} are used in the model [7, 22, 23] based on the dinuclear system concept [24]. Here $E_{\text{DNS}}^*(Z_P, A_P, \ell) = E_{\text{c.m.}} - V(Z_P, A_P, \ell, R_m)$ is the excitation energy of dinuclear system in the entrance channel, where Z_P and A_P are charge and mass numbers of the projectile nucleus. $V(Z, A, R_m, \ell)$ is the minimum value of the nucleus-nucleus potential well (for the DNS with charge asymmetry Z) and its position on the relative distance between the centers of nuclei is marked as $R = R_m$. The value of B_{qf} for the decay of DNS with the given charge asymmetry of fragments is equal to the depth of the potential well in the nuclear-nuclear interaction. The intrinsic fusion barrier B_{fus}^* is connected with mass (charge) asymmetry degree of freedom of the dinuclear system and it is determined from the potential energy surface:

$$U(Z; R, \ell) = U(Z, \ell, \beta_1, \alpha_1; \beta_2, \alpha_2) = B_1 + B_2 + V(Z, \ell, \beta_1, \alpha_1; \beta_2, \alpha_2; R) - (B_{\text{CN}} + V_{\text{CN}}(\ell)). \quad (11)$$

Here, B_1 , B_2 and B_{CN} are the binding energies of the nuclei in DNS and the CN, respectively, which were obtained from [25]; the fragment deformation parameters β_i are taken from the tables in [25–27] and α_i are the orientation angles of the reacting nuclei relative to the beam direction; $V_{\text{CN}}(\ell)$ is the rotational energy of the CN. The distribution of neutrons between two fragments for the given proton numbers Z and Z_2 or ratios A/Z and A_2/Z_2 for both fragments were determined by minimizing the potential $U(Z; R)$ as a function of A for each Z .

The driving potential $U_{\text{dr}}(Z) \equiv U(Z, R_m)$ is a curve linking minima in the potential well corresponding to each charge asymmetry Z in the valley of the potential energy surface from $Z = 0$ up to $Z = Z_{\text{CN}}$ as a function of the relative distance (see Fig. 4 of Ref. [2]). We define the intrinsic fusion barrier for the dinuclear system with charge asymmetry Z as $B_{\text{fus}}^*(Z, \ell) = U(Z_{\text{max}}, R_m(Z_{\text{max}}), \ell) - U(Z, R_m(Z), \ell)$, where $U(Z_{\text{max}}, \ell)$ is a maximum value of potential energy at $Z = Z_{\text{max}}$ in the valley along the way of complete fusion from the given Z configuration. The $B_{\text{sym}}^*(Z, \ell)$ is defined by the similar way as shown in Fig. 4 c of Ref. [2].

The masses and charges of the projectile and target nuclei are dynamical variables during capture and after formation of the DNS. The intense proton and neutron exchange between constituents of DNS is taken into account by calculation of the complete fusion probability P_{CN} as fusion from all populated DNS configurations according to the formula

$$P_{\text{CN}}(E_{\text{DNS}}^*(Z, A, \ell); \{\alpha_i\}) = \sum_{Z_{\text{sym}}}^{Z_{\text{max}}} Y_Z(E_{\text{DNS}}^*(Z, A, \ell)) P_{\text{CN}}^{(Z)}(E_{\text{DNS}}^*(Z, A, \ell); \{\alpha_i\}) \quad (12)$$

where $E_{\text{DNS}}^*(Z, A, \ell) = E_{\text{DNS}}^*(Z_P, A_P, \ell) + \Delta Q_{\text{gg}}(Z)$ is the excitation energy of DNS with angular momentum ℓ for a given value of its charge-asymmetry configuration Z and $Z_{\text{CN}} - Z$; $Z_{\text{sym}} = (Z_1 + Z_2)/2$; $\Delta Q_{\text{gg}}(Z)$ is the change of Q_{gg} -value by changing the charge (mass) asymmetry of DNS; $Y_Z(E_{\text{DNS}}^*(Z))$ is the probability of population of the $(Z, Z_{\text{CN}}-Z)$ configuration

at $E_{\text{DNS}}^{*(Z)}$ and given orientation angles (α_1, α_2) . $Y_Z(E_{\text{DNS}}^*, \ell, t)$ is the probability of population of the configuration $(Z, Z_{\text{tot}} - Z)$ at $E_{\text{DNS}}^*(Z)$ and ℓ . The evolution of Y_Z is calculated by solving the transport master equation:

$$\begin{aligned} \frac{\partial}{\partial t} Y_Z(E_Z^*, \ell, t) &= \Delta_{Z+1}^{(-)} Y_{Z+1}(E_Z^*, \ell, t) + \Delta_{Z-1}^{(+)} Y_{Z-1}(E_Z^*, \ell, t) \\ &\quad - (\Delta_Z^{(-)} + \Delta_Z^{(+)} + \Lambda_Z^{qf}) Y_Z(E_Z^*, \ell, t), \text{ for } Z = 2, 3, \dots, Z_{\text{tot}} - 2. \end{aligned} \quad (13)$$

Here, the transition coefficients of multinucleon transfer are calculated as in [18]

$$\Delta_Z^{(\pm)} = \frac{1}{\Delta t} \sum_{P,T} |g_{PT}^{(Z)}|^2 n_{T,P}^{(Z)}(t) (1 - n_{P,T}^{(Z)}(t)) \frac{\sin^2(\Delta t(\tilde{\varepsilon}_{P_Z} - \tilde{\varepsilon}_{T_Z})/2\hbar)}{(\tilde{\varepsilon}_{P_Z} - \tilde{\varepsilon}_{T_Z})^2/4}, \quad (14)$$

where the matrix elements g_{PT} describe one-nucleon exchange between the nuclei of DNS, and their values are calculated microscopically using the expression obtained in Ref. [28]. A non-equilibrium distribution of the excitation energy between the fragments was taken into account in calculations of the single-particle occupation numbers n_P and n_T as it was done in Ref. [29]; $\tilde{\varepsilon}_{P_Z}$ and $\tilde{\varepsilon}_{T_Z}$ are perturbed energies of single-particle states. In Eq. 13, Λ_Z^{qf} is the Kramers rate for the decay probability of the dinuclear system into two fragments with charge numbers Z and $Z_{\text{tot}} - Z$ (details in Ref. [30]), and it is proportional to $\exp(-B_{qf}(Z)/(kT))$ where $B_{qf}(Z)$ is the quasifission barrier.

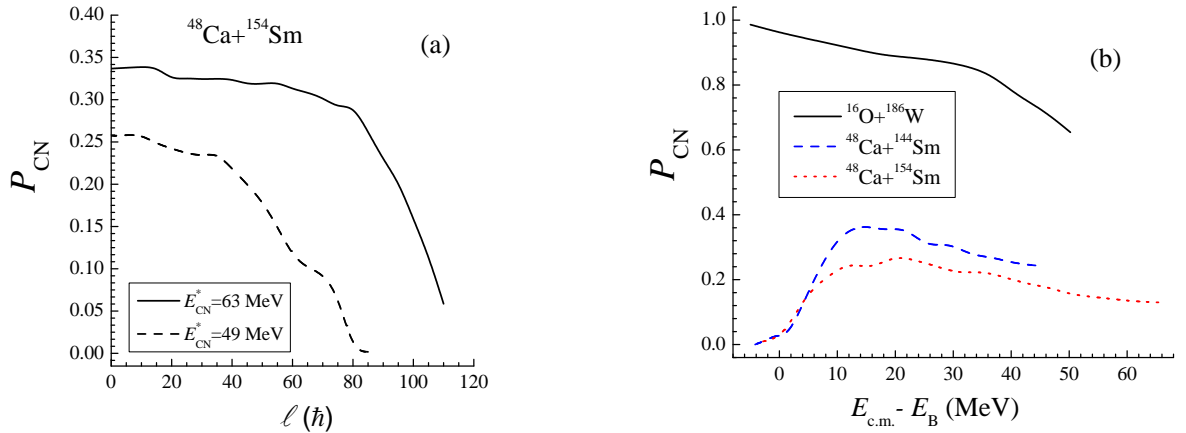


Figure 6. (a) The probability P_{CN} of compound nucleus formation as a function of the angular momentum of dinuclear system ℓ at energies $E_{\text{c.m.}} = 138$ and 154 MeV, corresponding to the excitation energies of the compound nucleus $E_{\text{CN}}^* = 49$ and 63 MeV. (b) The DNS model results for the fusion probability P_{CN} for the $^{16}\text{O} + ^{186}\text{W}$, $^{48}\text{Ca} + ^{144}\text{Sm}$ and $^{48}\text{Ca} + ^{154}\text{Sm}$ reactions as a function of the collision energy relative to the interaction barriers corresponding to each of reactions.

Eqs. (13) with the coefficients (14) and initial condition $Y_Z(E^*, 0) = \delta_{Z, Z_P}$ are solved numerically and the primary mass and charge distributions are found for a given interaction time $t_{\text{int}} = 5 \cdot 10^{-21}$ s (see Ref. [31]). In Eq. (12), we use the definition $Y_Z(E_Z^*, \ell) = Y_Z(E_Z^*, \ell, t_{\text{int}}(\ell))$. In (14) we use $\Delta t = 10^{-22}$ s $\ll t_{\text{int}}$.

As an example of our calculation of the fusion probability P_{CN} versus the angular momentum ℓ , we present the results for the $^{48}\text{Ca} + ^{154}\text{Sm}$ reaction at two different E_{CN}^* values (see Fig. 6 (a)) and the function P_{CN} versus the energy $E_{\text{c.m.}} - E_{\text{B}}$ for the reaction that lead to different

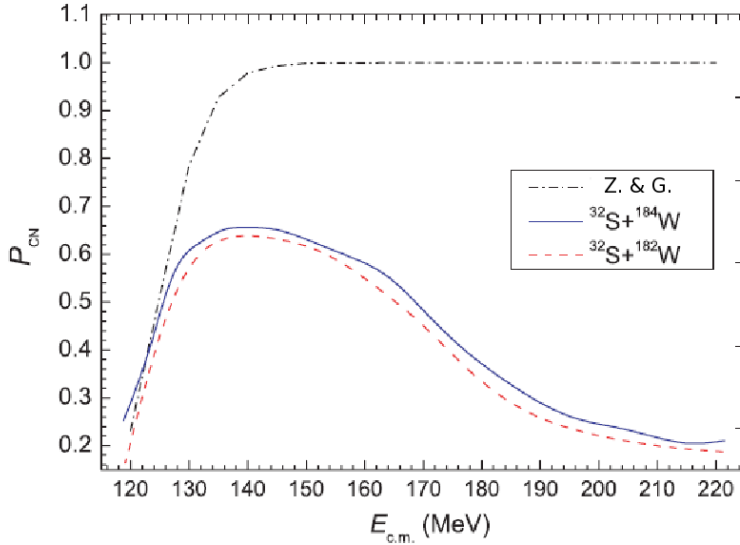


Figure 7. Our theoretical values of the fusion probability P_{CN} for the $^{32}\text{S}+^{184}\text{W}$ reaction as a function of collision energy $E_{\text{c.m.}}$, and the one of other authors (Z. & G.) of Ref. [8].

isotopes of thorium (see Fig. 6 (b)). This last figure shows the effect of the entrance channel on the P_{CN} fusion probability.

Moreover, Fig. 7 shows the calculation of P_{CN} as a function of the energy $E_{\text{c.m.}}$ for the two close $^{32}\text{S}+^{182}\text{W}$ and $^{32}\text{S}+^{184}\text{W}$ reactions for a wide range of excitation energies, in comparison with the calculation reported in Ref. [8]. For these two close reactions we observe two region of strong hindrance to fusion at very small and large values of the collision energy of $E_{\text{c.m.}}$ for both reactions while the approximate formula used in Ref. [8] gives similar results only at small energies, but P_{CN} increase quickly reaching a maximum value equal to 1 at $E_{\text{c.m.}} = 145$ MeV. In addition, there is no difference between the values of P_{CN} calculated by the approximated formula for the $^{32}\text{S}+^{182}\text{W}$ and $^{32}\text{S}+^{184}\text{W}$ reactions.

3.2. Compound Nucleus and Fast Fission contributions from the complete fusion formation

The branching ratio of the quasifission, fusion, and fast fission cross sections in formula (3) depend on the masses and charges, shell structure, mass asymmetry of projectile-target nuclei, as well as on the energy and impact parameter of heavy ion collision. As it was noted in Section 1, the formation of quasifission and fast fission products bypasses the stage of the CN formation. The difference between the two mentioned processes is in their dependence on the orbital angular momentum: quasifission is possible at all angular momenta of collision as fast fission occurs only at $\ell > \ell_f$, where ℓ_f is the angular momentum value at which the fission barrier of the compound nucleus disappears. The mass distributions of products of the capture reactions can be mixed by different proportions in different mass regions. To avoid ambiguity, the authors of Ref. [17] referred to the registered products as ones of the symmetric fragmentation (capture) because the genuine fission process is the decay of the compound nucleus into two fragments. The mass distribution of products of the fast fission reactions can be alike to that of the fusion-fission reactions. But the angular distribution of products of the former reaction is more anisotropic than that of the latter reaction due to the difference in their reaction time. In order to estimate the contribution of the fast fission into the calculated capture cross section, we use the value $\ell_f = 58$ obtained in Ref. [17] for the $^{48}\text{Ca}+^{208}\text{Pb}$ reaction.

In Fig. 8 the results of calculation for the fusion angular momentum distribution of this reaction is presented. One can see that maximum of the partial fusion cross section is around $\ell = 50$. The fast fission contribution for $\ell > \ell_f$ is calculated by formula (11), while the fusion cross section of CN must include the evaporation residues and fusion-fission cross sections only. In our calculation of evaporation residues, the values of the angular momentum $\ell < 58$ were used.

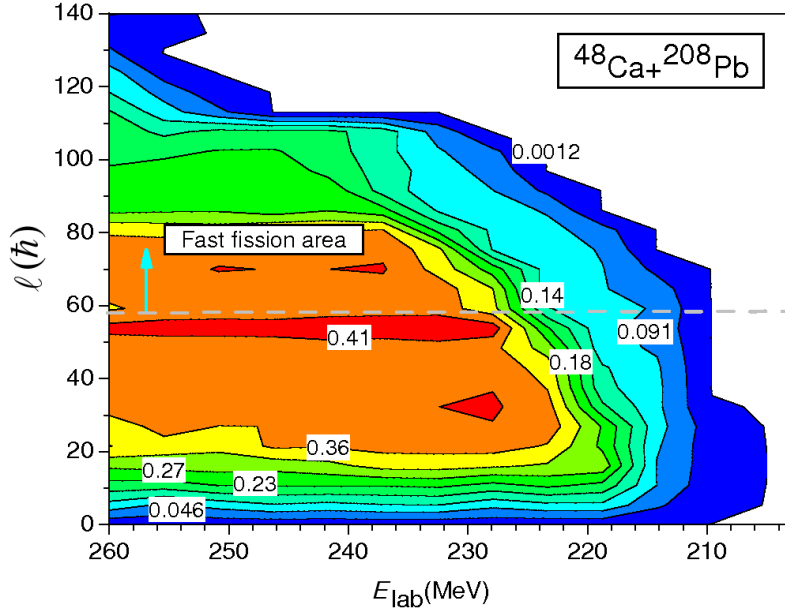


Figure 8. The results of calculation for the fusion angular momentum distribution of the $^{48}\text{Ca}+^{208}\text{Pb}$ reaction. The upper part of the figure, labelled by "Fast fission area", indicates the region where also the fast fission process appear.

3.3. Evaporation Residue

The probability of the formation of a evaporation residue nucleus surviving fission with mass number $A = A_{CN} - (\nu(x) + y(x) + 4k(x))$ and charge number $Z = Z_{CN} - (y(x) + 2k(x))$ from a heated and rotated compound nucleus $^{A_{CN}}Z_{CN}$ after emissions of ν neutrons, y protons, and k α -particles at the x th step of the de-excitation cascade is determined by the formula [6, 10]:

$$\sigma_{ER(x)}(E_x^*) = \sum_{\ell=0}^{\ell_f} (2\ell + 1) \sigma_{(x-1)}^{\ell}(E_x^*) W_{\text{sur}(x-1)}(E_x^*, \ell), \quad (15)$$

where $\sigma_{(x-1)}^{\ell}(E_x^*)$ is the partial cross section of the intermediate nucleus formation at the $(x-1)$ th step and $W_{\text{sur}(x-1)}(E_x^*, \ell)$ is the survival probability of the $(x-1)$ th intermediate nucleus against fission along the de-excitation cascade of CN; ℓ_f is the value of angular momentum ℓ at which the fission barrier for a compound nucleus disappears completely [21]; E_x^* is the excitation energy of the nucleus formed at the x th step of the de-excitation cascade. It is clear that $\sigma_{(0)}^{\ell}(E_0^*) = \sigma_{\text{fus}}^{\ell}(E_{CN}^*)$ at

$$E_{CN}^* = E_0^* = E_{\text{c.m.}} + Q_{gg} - E_{\text{rot}}, \quad (16)$$

where $E_{\text{c.m.}}$, Q_{gg} , and E_{rot} are the collision energy in the center of mass system, the reaction Q_{gg} -value, and rotational energy of the compound nucleus, respectively. The numbers of the emitted neutrons, protons, α -particles and γ -quanta, $\nu(x)n$, $y(x)p$, $k(x)\alpha$, and $s(x)\gamma$, respectively, are functions of the step x . The emission branching ratios of these particles depend on the excitation energy E_A^* and angular momentum ℓ_A of the cooling intermediate nucleus.

The de-excitation cascade, characterized by the emission of the above-mentioned particles, starts from the compound nucleus $^{A_{CN}}Z_{CN}$. Its formation probability is the partial cross section of complete fusion $\sigma_{\text{fus}}^{\ell}(E_{CN}^*)$ corresponding to the orbital angular momentum ℓ . The fusion cross section is equal to the capture cross section for light systems or light projectile-induced reactions, while for reactions with massive nuclei, it becomes a model-dependent quantity. Concerning estimation of the fusion cross section from the experimental fragments data, its value is sometimes an ambiguous quantity because of difficulties in separating the fusion-fission fragments from the quasifission fragments in the case of overlap of mass and angular distributions.

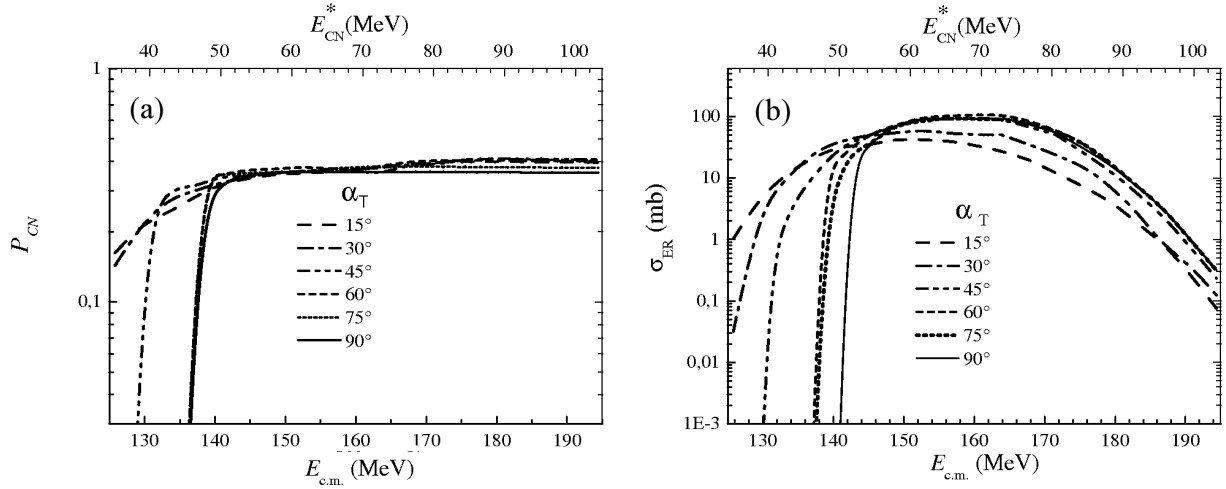


Figure 9. Fusion probability P_{CN} (a) versus the collision energy $E_{c.m.}$ for different values of the α_T angle. Evaporation residue cross sections (b) versus the $E_{c.m.}$ energy for various orientation angles α_T of the ^{154}Sm target.

As an example we present the results of our calculation for the $^{48}\text{Ca}+^{154}\text{Sm}$ reaction regarding the fusion probability P_{CN} (see Fig. 9 (a)) and evaporation residue cross sections σ_{ER} (see Fig. 9 (b)) as a function of the collision energy $E_{c.m.}$ for different values of the target orientation angles α_T . The dependence of the quasifission-fusion competition during the evolution of the dinuclear system and the sensitivity of the fission-evaporation competition during the de-excitation cascade of the compound nucleus on the values of orientation angle α_T are demonstrated. The analysis of the dependence of the compound nucleus and evaporation residue formation cross sections on α_T shows that the observed yield of evaporation residues in the $^{48}\text{Ca}+^{154}\text{Sm}$ reaction at the low energies ($E_{c.m.} < 137$ MeV) is formed in the collisions $\alpha_T < 45^\circ$. Because the initial beam energy is enough to overcome the corresponding Coulomb barrier for the collisions with these orientation angles α_T . Only in this case it is possible formation of dinuclear system which evolves to compound nucleus or breaks up into two fragments after multinucleon exchange without formation of the compound nucleus. At larger energies (about $E_{c.m.} = 140\text{--}180$ MeV) all orientation angles of the target-nucleus can contribute to σ_{ER} and its values are in the 10–100 mb range. At the larger collision energies ($E_{c.m.} > 158$ MeV) the complete fusion still increases but the evaporation residue cross section σ_{ER} goes down and its values are in the 1–0.1 mb range due to the strong decrease of the survival probability of the heated compound nucleus along de-excitation cascade. This is connected by the decrease of the fission barrier for a compound nucleus by increasing its excitation energy [1, 5] and angular momentum [21].

Another phenomenon leading to decrease of σ_{ER} at higher energy is the fast fission process which is the splitting of the mononucleus into two fragments due to absence of the fission barrier at very high the angular momentum $\ell > \ell_f$.

4. Mass distribution for quasifission and fusion-fission fragments at different energies

To show the importance of the overlap of mass distribution of quasifission and fusion-fission products in the unambiguous sorting out of events belonging to true fusion-fission process from the ones of quasifission process, we compare theoretical and experimental results of capture and fusion cross section for the $^{48}\text{Ca}+^{248}\text{Cm}$ reaction in Fig. 10 and discuss these results.

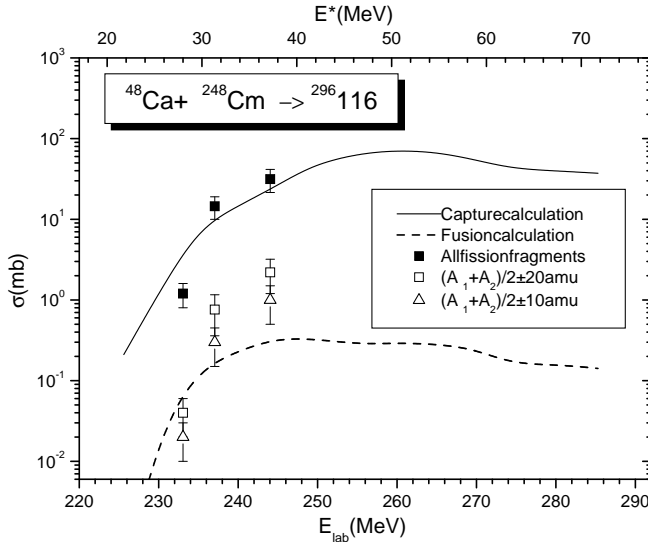


Figure 10. The capture and fusion cross section calculation, in comparison with the experimental data [32, 33], for the $^{48}\text{Ca} + ^{248}\text{Cm}$ reaction leading to the $^{296}116$ superheavy CN. The difference between the fusion cross section and more symmetric fragment yield $((A_1 + A_2)/2 \pm 10$ amu) at a higher excitation energy is related to the contribution of the quasifission process yielding more symmetric fragments.

The calculated capture cross section (solid line in Fig.10) is in good agreement with the experimental data [32] for the production of all fragments (full squares), while the theoretical fusion cross section (dashed line) is not in agreement with the experimental data obtained assuming the masses of the fusion-fission fragments belong in the ranges $(A_1 + A_2)/2 \pm 10$ or $((A_1 + A_2)/2 \pm 20$.

The presence of the quasifission contribution into measured fusion-fission cross section in the ranges under discussion causes disagreement with the theoretical results. If it is assumed that the experimental fusion - fission events are in the $(A_1 + A_2)/2 \pm 10$ amu interval (almost close to the $\sqrt{(A_1 + A_2)/2}$ value), the calculated fusion cross sections (the dashed line) will be closer to the new set of the experimental data (open triangles [33] in Fig.10). Indeed, in this case there is an appreciable contribution of the quasifission process (or a contribution which cannot be neglected), in addition to the fusion-fission fragment formation. Therefore, the estimated experimental fusion cross section, connected with the new set of the experimental events of fission fragments, still appears to be a little larger than the calculated fusion excitation function at higher excitation energies. A preliminary calculation of the mass distribution of quasifission fragments for a fixed reaction time t_{reac} of a DNS performed in the framework of the model developed on the basis of the dinuclear system concept [34, 35], indicates that the fragments of the quasifission process also appear in the mass-symmetric region and are mixed with the fragments coming from the fusion-fission process.

5. Study of the reaction dynamics of two close mass asymmetric reactions by the analysis of the fusion-evaporation and fusion-fission processes

There are three main processes causing hindrances to ER formation in reactions with massive nuclei: quasifission, fusion-fission, and fast fission [13]. All of these processes produce binary fragments in different stages of reaction. Moreover, the angular and mass distributions of some parts of their products can overlap [13, 36]. Ignoring this mixing may lead to ambiguity at analysis of the experimental data connected with the binary fragments. This problem should be studied carefully.

The ER formation process is often considered as the third stage of the three-stage process. The first stage is capture-formation of the DNS after full momentum transfer into the deformation energy of nuclei, their excitation energy, and rotational energy from the initial relative motion of the colliding heavy ions in the center-of-mass system. Capture takes place

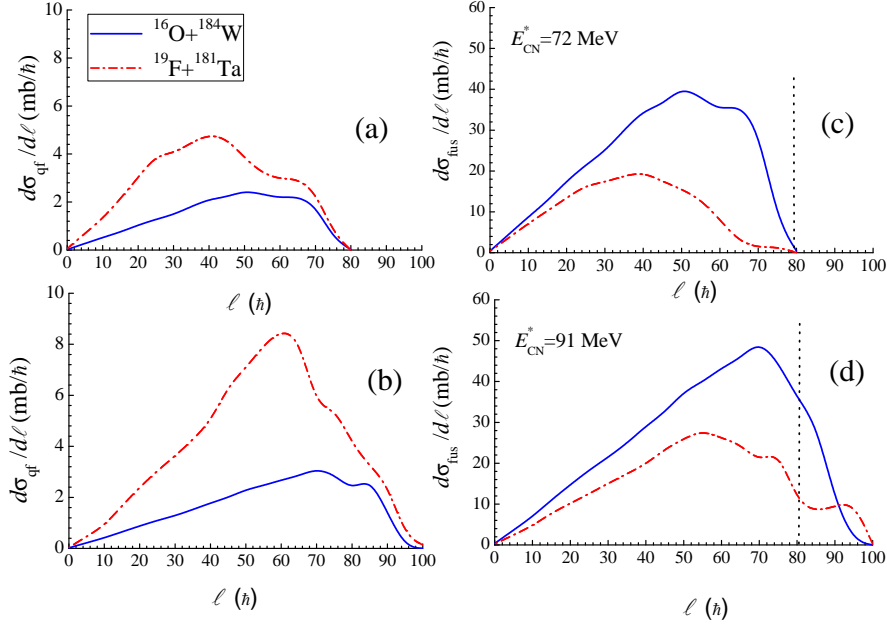


Figure 11. Partial quasifission ((a) and (b) panels) and fusion ((c) and (d) panels) cross sections as a function of the angular momentum ℓ for the $^{16}\text{O}+^{184}\text{W}$ (solid line) and $^{19}\text{F}+^{181}\text{Ta}$ (dashed line) reactions. In the panel (a) the beam energies of reactions induced by ^{16}O and ^{19}F are $E_{\text{c.m.}} = 96.2$ MeV and 95.7 MeV, respectively. These energies correspond to the same excitation energy of CN $E_{\text{CN}}^* = 72$ MeV for the both systems shown in the panel (c). Analogously, in the panel (b) the beam energies are $E_{\text{c.m.}} = 115.2$ MeV and $E_{\text{c.m.}} = 114.7$ MeV, respectively. The corresponding excitation energy of CN is 91 MeV shown in the panel (d). In (c) and (d), the vertical dashed line at $\ell_f = 80\hbar$ separates compound nucleus and fast fission contributions.

if the initial energy of the projectile in the center-of-mass system is enough to overcome the interaction barrier (Coulomb barrier + rotational energy of the entrance channel) [22]. The study of the dynamics of heavy ion collisions at energies near the Coulomb barrier shows that complete fusion does not occur immediately in collisions of massive nuclei [1, 13, 23, 37, 38]. After formation of the DNS, the quasifission process competes with the formation of CN. Quasifission occurs when the DNS prefers to break down into fragments instead of being transformed into a fully equilibrated CN. The number of events contributing to quasifission increases drastically by increasing the sum of the Coulomb interaction and rotational energy in the entrance channel [3, 7, 9].

Another reason for the decreasing yield of ER with increasing excitation energies is the usual fission of a heated and rotating CN that was formed in competition with quasifission. The stability of a massive CN decreases due to the decrease in the fission barrier by increasing its excitation energy E_{CN}^* and angular momentum ℓ [39–41]. The theoretical values of the quasifission partial cross sections for the $^{19}\text{F}+^{181}\text{Ta}$ and $^{16}\text{O}+^{184}\text{W}$ reactions are presented in the left panels of Fig. 11. It is seen from these figures that the quasifission takes place at all values of ℓ leading to capture. The angular momentum distributions of CN formed in these reactions at the excitation energies $E_{\text{CN}}^* = 72$ and 91 MeV are presented in the right panels of Fig. 11. The spin distributions of CN formed in each of these reactions differ mainly by the probability but not by the values of the angular momentum ranges. This means that the number of CN formed in both reactions under discussion are different, but they have a similar range of the angular momentum ℓ . The vertical dotted lines at $\ell_f = 80\hbar$ in these panels separates the

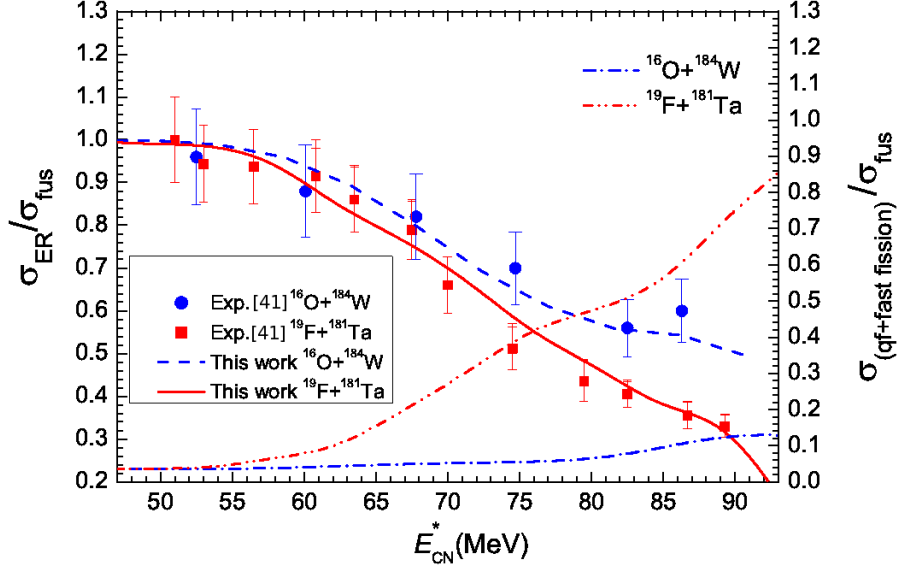


Figure 12. Comparison of the experimental values of the evaporation residue cross sections normalized with respect to the capture cross sections for the $^{16}\text{O}+^{184}\text{W}$ (solid circles) [42] and $^{19}\text{F}+^{181}\text{Ta}$ systems (solid squares) [42] with the corresponding theoretical results (dashed and solid lines, respectively) as a function of the excitation energy E_{CN}^* of CN (left axis). Theoretical results of the sum of the quasifission and fast fission cross sections (normalized with respect of the fusion cross sections) for the $^{16}\text{O}+^{184}\text{W}$ (dot dashed line) and $^{19}\text{F}+^{181}\text{Ta}$ (dot-dot dashed line) systems are presented versus E_{CN}^* and compared on the right axis.

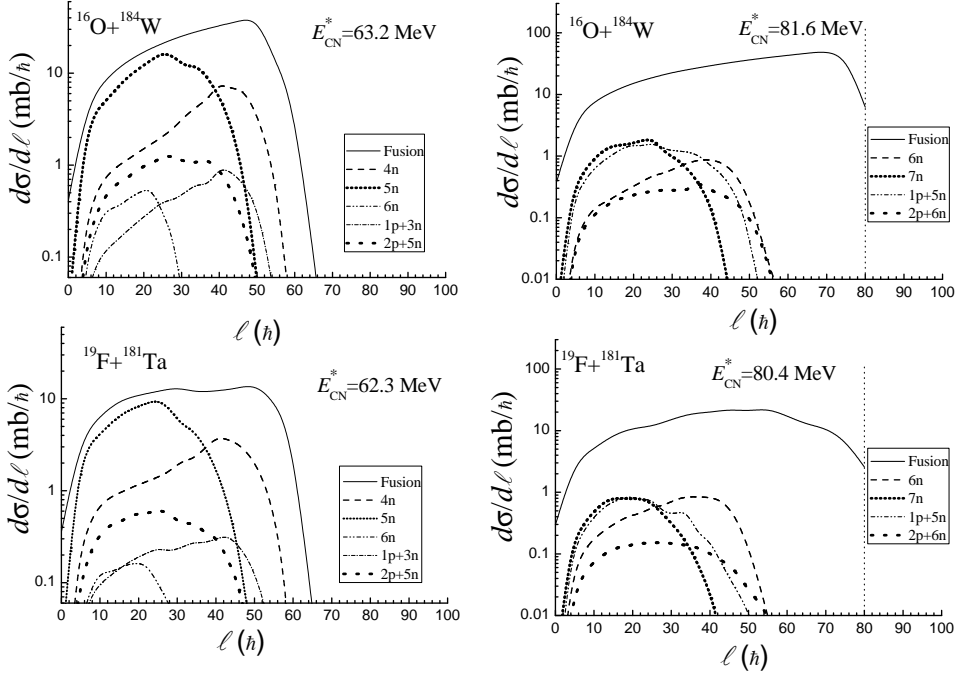


Figure 13. Spin distribution of evaporation residue cross sections as a function of the angular momentum ℓ . The upper part is for the $^{16}\text{O}+^{184}\text{W}$ reaction, the lower part is for $^{19}\text{F}+^{181}\text{Ta}$ reaction, both at two E_{CN}^* energies: approximately 62-63 MeV and 80-81 MeV.

complete fusion ($\ell_f < 80\hbar$) and fast fission ($\ell_f \geq 80\hbar$) regions of the angular momentum.

The quasifission and fast fission processes produce binary fragments which can overlap with

those of the fusion-fission channel and the amount of mixed detected fragments depends on the mass asymmetry of entrance channel, as well as on the shell structure of the reaction fragments being formed. The suggestion for the experimental studies of the difference between characteristics of the fusion-fission, quasifission and fast fission products can be made when their mass (charge), kinetic energy and angular distributions are explored in detail by dynamical calculations allowing to obtain the relaxation times of these processes. Therefore, the correct estimation of the CN formation probability in the reactions with massive nuclei is a difficult task for both experimentalists and theorists. Different assumptions about the fusion process are used in different theoretical models which can give different cross sections. The experimental methods used to estimate the fusion probability depend on an unambiguous identification of the complete fusion products among the quasifission products. The difficulties arise when the mass (charge) and angular distributions of the quasifission and fusion-fission fragments strongly overlap, depending on the reaction dynamics. As a result, the complete fusion cross sections may be overestimated [9].

We confirm that the compared ratios of the cross sections between evaporation residues and complete fusion σ_{ER}/σ_{fus} for the $^{16}\text{O}+^{184}\text{W}$ and $^{19}\text{F}+^{181}\text{Ta}$ reactions discussed in [42] are not free from the above-mentioned ambiguity in the determination of the fusion cross section σ_{fus} . Theoretical values of the fusion cross section include only evaporation residues and fusion-fission cross sections

$$\sigma_{fus} = \sigma_{ER} + \sigma_{ff}. \quad (17)$$

The experimental values of fusion cross section reconstructed from the detected fissionlike fragments and evaporation residues [42]:

$$\sigma_{fus}^{(exp)} = \sigma_{ff} + \sigma_{qf} + \sigma_{fast\ fission} + \sigma_{ER}, \quad (18)$$

where σ_{ff} , σ_{qf} , and $\sigma_{fast\ fission}$ are the contributions of fusion-fission, quasifission and fast fission processes, respectively, and σ_{ER} is the ER contribution. According to the statement of the authors of Ref. [42], the complete fusion cross sections are obtained by adding fission cross sections [43] to the measured data of the evaporation residue cross sections [44]. Therefore, we can state that the definition of the experimental fusion cross section is similar with the definition of capture [9]: $\sigma_{fus}^{(exp)} = \sigma_{cap}$.

In Ref. [43], the complete fusion cross section is derived from a statistical model where only neutron evaporation and fission are included. We think that the fission data from Ref. [43] contain quasifission fragments and, at larger beam energies, also fast fission contributions, which appear as hindrances to complete fusion. This argument is confirmed by our results obtained in the framework of the DNS model. We calculate the total ER and fusion-fission excitation functions in the framework of the advanced statistical model [39–41].

6. Study for the synthesis of the $^{297}\text{117}$ element by the $^{48}\text{Ca}+^{249}\text{Bk}$ reaction

By using the above-mentioned method we calculated the capture, quasifission, fast fission and fusion (formation of CN) cross sections for the ^{48}Ca induced reaction on the ^{249}Bk target (see Fig. 14 (b)). In the $E_{c.m.} < 200$ MeV energy range the fusion cross section is about three orders of magnitude lower than that of quasifission (which is close to the capture cross section in the whole explored energy range), and it is about one order of magnitude lower than the one of fast fission. At higher $E_{c.m.}$ energies, the fusion cross section is about two orders of magnitude lower than that of quasifission, while it is about five times lower than the one of fast fission. In this reaction the quasifission is the completely dominant process in comparison to complete fusion, and the fast fission is also a strongly relevant process in comparison to the fusion formation (CN). In this case, fast fission process takes place starting from the ℓ_f value equal to $30 \hbar$.

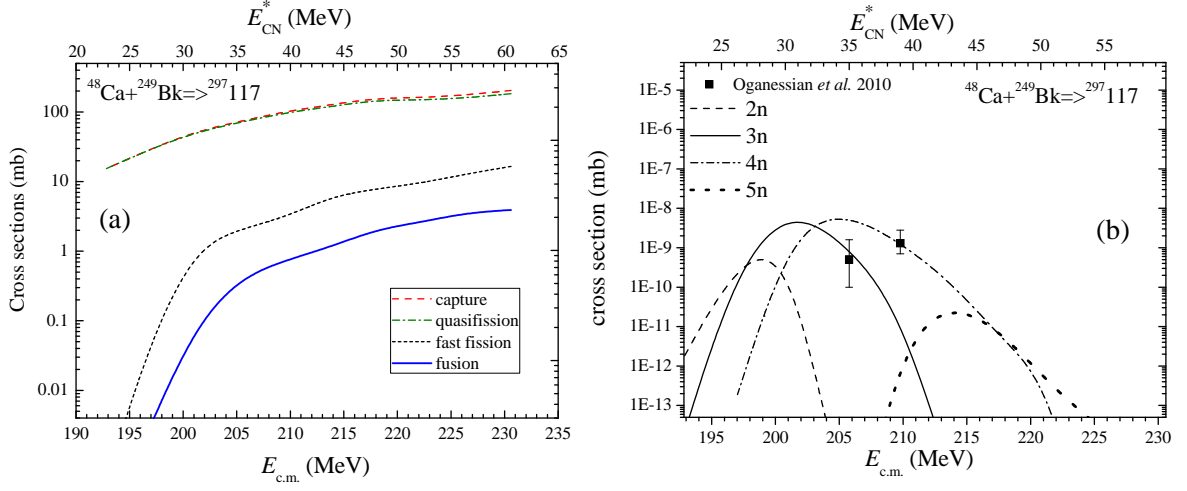


Figure 14. (a) Capture, quasifission, fast fission, and fusion cross sections for the $^{48}\text{Ca}+^{249}\text{Bk}$ reaction leading to $^{297}\text{117}$ compound nucleus as a function of the colliding energy $E_{c.m.}$. (b) Evaporation residue cross sections, after neutron emission only, calculated for the $^{48}\text{Ca}+^{249}\text{Bk}$ reaction leading to $^{297}\text{117}$ compound nucleus as a function of the colliding energy $E_{c.m.}$, in comparison with the experimental data (full square) presented in Ref. [48].

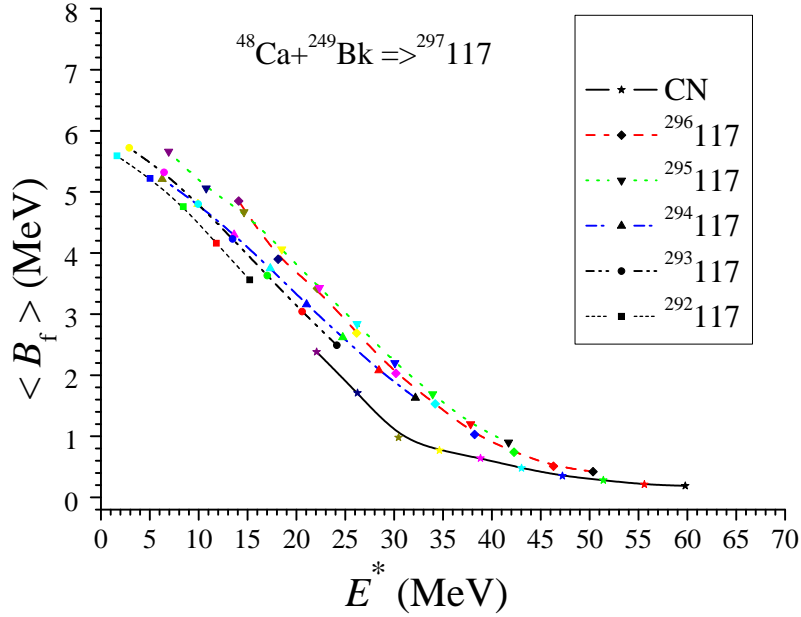


Figure 15. The effective fission barrier $\langle B_f \rangle$ as a function of the excitation energy for the $^{48}\text{Ca}+^{249}\text{Bk}$ reaction leading to $^{297}\text{117}$ compound nucleus.

The shell corrections for the odd-odd and odd-even nuclei in the 292-297 mass region of the 117 element were obtained from the static fission barrier B_f (for $\ell=0$) calculated by Sobiczewski [45], which correspond to the realistic values of shell corrections, as an extension of the results presented in the paper of Kowal *et al.* [46] for the even-even superheavy nuclei. We calculated the average effective fission barriers and evaporation residue cross sections for all nuclei along the de-excitation cascade of the $^{297}\text{117}$ compound nucleus by using such values of shell corrections (for $\ell=0$) and taking into account their fade-out (see Refs. [1,6,10,47] and references therein) as

a function of the temperature and angular momentum. In Fig. 14(b), we compare the individual excitation functions of the evaporation residue for emission of neutron only along the cascade of CN with ER cross sections after 3n and 4n emission from CN measured by Oganessian *et al.* in their experiment [48]. As one can see our result are in good agreement with the experimental data and we also find that the peaks of such excitation functions for 3n and 4n emission are present at about 30.6 and 34.0 MeV, respectively. The maximum yield of the 2n contribution (5×10^{-1} pb) is lower than the ones of the 3n and 4n contributions. The maximum yield of the 5n contribution is about 2.3×10^{-2} pb at $E_{CN}^* = 43.2$ MeV. Moreover, in Fig. 15 we report the effective fission barrier $\langle B_f \rangle$ distribution as a function of E^* along the cascade of CN at different excitation energies and neutron number of the intermediate excited nuclei.

In Table 1 are reported such $\langle B_f \rangle$ values obtained for the chain of nuclei, at three different E^* values of the considered excited nuclei. In Table 1 the rows show the evolution of the effective

Table 1. Effective fission barrier $\langle B_f \rangle$ for the $^{48}\text{Ca}+^{249}\text{Bk} \rightarrow ^{297}117$ reaction leading to intermediate excited nuclei with masses $A=297, 296, 295, 294, 293$ and 292 , at excitation energies of nuclei $E^*=17, 25$ and 33 MeV.

E^* (MeV)	A= 297 N= 180	A= 296 N= 179	A= 295 N= 175	A= 294 N= 177	A= 293 N= 176	A= 292 N= 175
17	4.2	4.3	3.8	3.6	3.3
25	1.9	2.9	3.0	2.6	2.4
33	0.8	1.7	1.8	1.6

fission barrier $\langle B_f \rangle$ values for different neutron number of excited nuclei when they are formed with a defined excitation energy E^* (for example 17, 25, 33 MeV). Of course, such conditions for the intermediate nuclei are reached starting from different excitation energy values of E_{CN}^* . In details, to form the nuclei with masses A of 297, 296, 295, 294 and 293 u at the same excitation energy, for example $E^*=25$ MeV, it is necessary to start from CN with excitation energy of 25.0, 33.5, 41.7, 51.6 and 60.8 MeV, respectively. The changing of the $\langle B_f \rangle$ values along the rows are related to the structure effects of nuclei by changing the neutron number. Such changes of $\langle B_f \rangle$ are similar for the three presented cases of excitation energies. Instead, the $\langle B_f \rangle$ values along a column show the change of the effective fission barrier for a defined intermediate nucleus by changing its excitation energy E^* . For all intermediate nuclei with different neutron number, the changes have the same trend by changing the excitation energy E^* . It is clear that the $\langle B_f \rangle$ value decreases increasing E^* .

7. Conclusions

In the large number of capture reactions with massive nuclei the quasifission process with its peculiarities is the main subject for the understanding of the reaction dynamics. Therefore, the intense yield of quasifission fragments dominates in the reactions with ^{124}Sn and ^{132}Sn (neutron-rich) beams with targets heavier than ^{92}Zr , and in the reactions with the Coulomb parameter $z = \frac{Z_1 \times Z_2}{A_1^{1/3} + A_2^{1/3}}$ (connected with the intense Coulomb repulsion between reacting nuclei) higher than 200, for which the quasifission yield is at least two orders of magnitude higher than the complete fusion yield (and then the fusion probability P_{CN} is lower than about 10^{-2} , as for example for the reactions listed in Table 2).

So, all above-mentioned reactions are excellent reactions for the study of the quasifission process. For the last reaction ($^{238}\text{U}+^{248}\text{Cm}$) in Table 2 the P_{CN} value is not reported because for this reaction capture cross section does not exist.

Table 2. Reactions, total Z of the system, z parameter of the Coulomb repulsion, and fusion probability P_{CN} are reported.

Reaction	Z_{tot}	$z = \frac{Z_1 \times Z_2}{A_1^{1/3} + A_2^{1/3}}$	P_{CN}
$^{86}\text{Kr} + ^{136}\text{Xe}$	90	204	$\sim 4 \times 10^{-2}$
$^{92}\text{Zr} + ^{132}\text{Sn}$	90	209	$\sim 5 \times 10^{-2}$
$^{136}\text{Xe} + ^{136}\text{Xe}$	108	284	$< 10^{-10}$
$^{64}\text{Ni} + ^{208}\text{Pb}$	110	232	$< 10^{-5}$
$^{208}\text{Pb} + ^{70}\text{Ge}$	114	262	$< 10^{-7}$
$^{139,149}\text{La} + ^{139,149}\text{La}$	114	306, 317	$< 10^{-10}$
$^{86}\text{Kr} + ^{208}\text{Pb}$	118	286	$< 10^{-7}$
$^{238}\text{U} + ^{58}\text{Ni}$	120	256	$< 10^{-6}$
$^{132}\text{Sn} + ^{174}\text{Yb}$	120	327	$< 10^{-10}$
$^{238}\text{U} + ^{70}\text{Ge}$	124	286	$< 10^{-7}$
$^{58}\text{Fe} + ^{249}\text{Cf}$	124	251	$< 10^{-3}$
$^{132}\text{Sn} + ^{186}\text{W}$	124	343	$< 10^{-11}$
$^{132}\text{Sn} + ^{208}\text{Pb}$	132	373	$< 10^{-13}$
$^{160}\text{Gd} + ^{186}\text{W}$	138	431	$< 10^{-16}$
$^{132}\text{Sn} + ^{249}\text{Cf}$	148	430	$< 10^{-15}$
$^{238}\text{U} + ^{248}\text{Cm}$	188	707	-----

Moreover, at energies higher than the Coulomb barrier, the fast fission process gives a relevant contribution to formation of fissionlike fragments. For these reactions the contribution of the complete fusion cross section to the capture cross section is very small. Consequently, the ER cross section is very small too, or in many cases is lower than the limit (about 0.2 pb) of the present possibility of the experimental setup. Therefore, it is necessary to estimate the quasifission, fast fission and complete fusion cross sections by a hopeful analysis of the reaction dynamics before to plan new long beam-time and expensive experiments. Because only the fusion-fission and fusion-evaporation yields contribute to the complete fusion cross section. Only in the two above-mentioned reactions ($^{92}\text{Zr} + ^{132}\text{Sn}$, $^{86}\text{Kr} + ^{136}\text{Xe}$) it is possible to observe evaporation residues. For all other reactions listed in Table 2 it is not possible to observe meaningful fusion-fission contributions and least of all evaporation residues. The ratio of fusion-fission and quasifission fragment yields for the all other mentioned reactions are much lower than 10^{-3} . Therefore it is impossible to separate the fragments of fusion-fission process from the fragments of the huge amount of quasifission process. Our theoretical model is a powerful predictive method to calculate the yield of reaction products and also to describe the processes in the reactions with massive nuclei. Moreover, also for reactions used to synthesis of superheavy elements our model is able to calculate the effective fission barriers along the various steps of the de-excitation cascade with the neutron and proton emission from the compound nucleus and intermediate excited nuclear systems at various excitation energy and angular momentum.

References

- [1] Fazio G *et al.* 2004 *Eur. Phys. J. A* **19** 89
- [2] Zhang H Q *et al.* 2010 *Phys. Rev C* **81** 034611
- [3] Giardina G *et al.* 2000 *Eur. Phys. J. A* **8** 205
- [4] Giardina G *et al.* 2000 *Nucl. Phys A* **671** 165
- [5] Fazio G *et al.* 2003 *J. Phys. Soc. Jpn.* **72** 2509
- [6] Fazio G *et al.* 2004 *Eur. Phys. J. A* **22** 75
- [7] Fazio G *et al.* 2005 *Phys. Rev C* **72** 064614

- [8] Zagrebaev V and Greiner W *et al.* 2008 *Phys. Rev C* **78** 034610
- [9] Oganessian Yu. *et al.* 2009 *Phys. Rev C* **79** 024608
- [10] Fazio G *et al.* 2005 *Mod. Phys. Lett. A* **20** 391
- [11] Fazio G *et al.* 2008 *J. Phys. Soc. Jpn.* **77** 2509
- [12] Nasirov A K *et al.* 2009 *Int. J. Mod. Phys. E* **18** 841
- [13] Nasirov A K *et al.* 2009 *Phys. Rev C* **79** 024606
- [14] Nasirov A K *et al.* 2010 *Phys. Lett. B* **686** 72
- [15] Nasirov A K *et al.* 2010 *J. Phys: Conf. Ser.* **205** 012018
- [16] Itkis M G *et al.* 2004 *Acta Phys. Hung. A* **19** 9
- [17] Bock R *et al.* 1982 *Nucl Phys. A* **388** 334
- [18] Jolos R V *et al.* 1986 *Sov. J. Nucl. Phys.* **44** 228
- [19] Nasirov A K *et al.* 2004 *Acta Phys. Hung. A* **19** 109
- [20] G.N. Knyazheva, E.M. Kozulin, R.N. Sagaidak, A.Yu. Chizhov, M.G. Itkis, N.A. Kondratiev, V. M. Voskressensky, M. Stefanini, B.R. Behera, L. Corradi, *Phys. Rev. C* **75** (2007) 064602.
- [21] Sierk A J 1986 *Phys. Rev. C* **33** 2039
- [22] Nasirov A K *et al.* 2005 *Nucl. Phys. A* **759** 342
- [23] Adamian G G *et al.* 2003 *Phys. Rev. C* **68** 034601
- [24] Volkov V V in *Contributed Papers of Nucleus-Nucleus Collision II, Visby, 1985*, edited by B. Jakobson and K. Aleclett (North-Holland, Amsterdam, 1985), Vol.1, p.54; *Izv. Akad. Nauk SSSR Ser. Fiz.* 50, 1879 (1986); in *Proceedings of International School-Seminar on Heavy Ion Physics, Dubna, 1986, D7-87-68 (Dubna, 1987)*, p. 528; in *Proceedings of the 6th International Conference on Nuclear Reaction Mechanisms, Varenna, 1991*, edited by E. Gadioli (*Ricerca Scientifica ed Educazione Permanente Supplemento n.84, 1991*), p.39. on *Heavy Ion Physics*
- [25] Moller P and Nix J R 1988 *Atomic Data and Nuclear Data* **39** 213
- [26] Raman S *et al.* 1987 *Atomic Data and Nuclear Data* **36** 1
- [27] Spear R H 1989 *Atomic Data and Nuclear Data* **42** 55
- [28] Adamian G G *et al.* 1992 *Sov. J. Nucl. Phys.* **55** 660
- [29] Adamian G G *et al.* 1994 *Z. Phys. A* **347** 203
- [30] Adamian G G *et al.* 2003 *Phys. Rev. C* **68** 034601
- [31] Töke J *et al.* 1985 *Nucl. Phys. A* **440** 327
- [32] Itkis M G *et al.* 2002 *Proc. of the International Conference on Nuclear Physics at Border Lines, May 21-24, 2001 Lipari (Messina), Italy*, eds. G.Fazio, G.Giardina, F.Hanappe, G.Imme, N.Rowley. World Scientific, Singapore, p.146-156
- [33] Kozulin E 2002 private communication
- [34] Dzholos R V *et al.* 1989 *Sov. J. Nucl. Phys.* **50** 382
- [35] Fazio G *et al.* 2003 *Proc. of the International Symposium on New Projects and Lines of Research in Nuclear Physics, October 24-26, 2002, Messina, Italy*, eds. G.Fazio, F.Hanappe. World Scientific, Singapore, p.258-271
- [36] Nasirov A K *et al.* 2007 *Eur. Phys. J. A* **34** 325
- [37] Back B B 1985 *Phys. Rev. C* **31** 2104
- [38] Antonenko N A *et al.* 1995 *Phys. Rev. C* **51** 2635
- [39] D' Arrigo A *et al.* 1992 *Phys. Rev. C* **46** 1437
- [40] D' Arrigo A *et al.* 1994 *J. Phys. G* **20** 365
- [41] Sagaidak R N *et al.* 1998 *J. Phys. G* **24** 611
- [42] Shidling P D *et al.* 2008 *Phys. Lett. B* **670** 99
- [43] Forster J S *et al.* 1987 *Nucl. Phys. A* **464** 497
- [44] Hinde D J *et al.* 1982 *Nucl. Phys. A* **385** 109
- [45] Sobiczewski A 2011 private communication
- [46] Kowal M *et al.* 2010 *Phys Rev C* **82** 014303
- [47] Drozdov V *et al.* 2003 *J. Phys. Soc. Jpn.* **72** 2118
- [48] Oganessian Yu Ts *et al.* 2010 *Phys. Rev. Lett* **104** 142502